

AN ELECTROSTATIC FIXED-SLIT EMITTANCE MEASUREMENT SYSTEM*

J.W. Lewellen[†], H.L. Andrews, R.L. Fleming, K. Nichols, E.I. Simakov,
 Los Alamos National Laboratory, Los Alamos, USA

Abstract

The emittance of a field emission cathode can be difficult to measure close to the emitter, due to the high average current density of the beam and the potential for desorbed material from an imaging screen to contaminate the cathode. We present the design for a dual fixed-slit emittance measurement system for a field emitter cathode, implemented using electrostatic deflecting plates.

INTRODUCTION

Los Alamos National Laboratory is engaged in the development of a laser accelerator based upon the additive manufacture of a dielectric structure [1]. A key feature is the use of diamond pyramid field emitters (DFEs) [2-4], operated at 10-40 kV, as the beam source.

The beams from DFEs, like many field emitters, appear to have outstanding emittance; however, the large beam divergence, measured to be on the order of 5 – 10 degrees [5], presents challenges for capturing and focusing the beam into the DLA structure, as well as for characterizing the beam properties, specifically the beam emittance.

A simple variable-focus permanent-magnet solenoid-like lens has been developed to provide for initial focusing and is described in [6]. We have also designed a dual-slit emittance measurement system to characterize the (focused) beam using a non-imaging technique and with the measurement point a significant distance from the cathode; this helps to avoid contaminating the cathode from “blow-back” of desorbed material.

In principle our approach is similar to the Cornell dual-slit method, implemented using beam steering magnets [7]; differences, other than the beam energy, include the use of electrostatic rather than magnetic deflectors, and a minimal drift distance between deflectors.

DESIGN BASICS

One of the main attractions of a dual-slit emittance measurement system is the ability to obtain a transverse phase-space density map, as opposed to a simple RMS value. Also, the measurement is performed without requiring optical imaging of low-emittance beams.

Ideally, an emittance mapper would be built using two co-located slits transverse to the direction of beam propagation, one in real space and one in momentum space; by translating the slits across the beam, the phase space could be sampled, at a resolution set by the widths of the slits, by simply measuring the transmitted beam current or charge

as a function of slit position. Unfortunately, fabricating a momentum-space slit is quite challenging; but by using a real-space slit followed by a drift and a second real-space slit, we can build a reasonable approximation.

The process is illustrated in Figure 1.

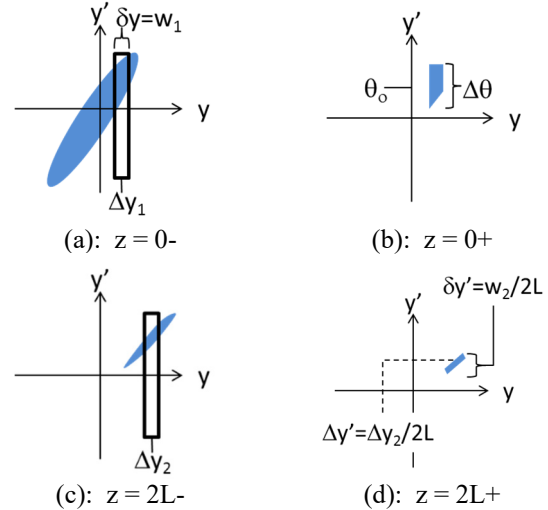


Figure 1: Dual slit-based phase space measurement, where “-” and “+” indicate immediately before or after a slit, respectively.

First, a real-space slit of width w_1 (smaller than the beam spot size at the slit), located longitudinally at $z=0$ and transversely at Δy_1 , slices a beamlet out of an on-axis and diverging beam. The phase space just before and just after the first slit is shown in Fig. 1(a) and (b), respectively. The beamlet thus produced is by definition at a waist, with a width $\delta y = w_1$ and angular spread $\Delta \theta$.

The beamlet’s centroid will propagate at angle θ_0 with respect to the z axis, with θ_0 depending on Δy_1 (location of the slit) and properties of the beam at the slit. As it propagates the beamlet diverges with an opening angle of $\Delta \theta$. The beamlet is allowed to drift for a distance $2L$. A second slit of width w_2 , located at $z=2L$, again generates a beamlet as shown in Fig. 1(c) and (d). The width of the second slit, combined with the drift distance, represents an angular acceptance $\delta y' = w_2/2L$ (given $w_2 \ll 2L$), while the location of the second slit, combined with the drift distance, provides an angular position $\Delta y' = \Delta y_2/2L$. So long as the divergence of the beamlet $\Delta \theta$ is larger than the angular acceptance $\delta y'$, by moving the two slits and measuring the transmitted current (or charge) we can determine the transverse phase-space density of the beam to a spatial (angular) resolution of δy ($\delta y'$).

While this description assumes the slits move, in practice we choose to translate the beam and beamlet over fixed-

Content from this work may be used under the terms of the CC BY 3.0 licence (© 2018). Any distribution of this work must maintain attribution to the author(s), title of the work, publisher, and DOI.

* Work supported by the Los Alamos National Laboratory LDRD program.

[†] jwlewellen@lanl.gov

position slits using a pair of electrostatic translators described in this paper.

ELECTROSTATIC MODEL

Basic Principles

The building block of our emittance measurement system is an electrostatic translator made from parallel-plate capacitors, as illustrated in Figure 2. V_p is the net voltage applied across a plate pair; L is the length of a plate; g is the vertical gap between the plates; and w is the width of the exit slit. An electron beam entering the beam scanner from the left ($z=0$) can be characterized as having an initial transverse offset x_i and direction θ_i . Electrons in the beam will have transverse and longitudinal velocities $v_{xi(z)}$. For most reasonable beams we can assume $v_{xi} \ll v_{zi}$, and in the energy range of interest, the beam is non-relativistic, e.g. $v_{zi} \approx \sqrt{2qV_b/m} \ll c$, where q is the electronic charge, m is the electron rest mass, c is the speed of light, and V_b is the beam voltage.

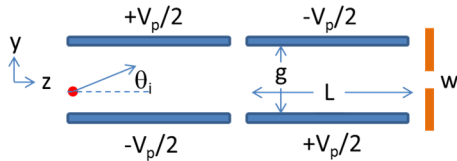


Figure 2: Schematic of an electrostatic translator.

At the end of the translator, assuming the longitudinal gaps between the plates are negligible and the electric field along the axis of deflection, $E_y(z)$, is sinusoidal (i.e. $L \sim g$) with a period of $2L$ and peak of V_p/g , the transverse beam position at the exit slit is given by

$$y_f = y_i + 2L\theta_i + \frac{1}{\pi} \frac{L^2 V_p}{g V_b}. \quad (1)$$

For instance, given a plate length L of 1 cm, a gap of 1 cm, and a plate voltage V_p of 1 kV, a 40-keV beam will be offset by $80 \mu\text{m}$ at the slit from its undeflected position. The power supply resolution should be

$$\Delta V_p \leq \frac{\pi g w V_b}{L^2} \quad (2)$$

in order to scan the beam in increments of one slit width, and jitter should ideally be a small fraction of the resolution.

Constraints

The smaller the gap g , the lower the voltage V_p required to achieve a given deflection, so there is incentive to minimize g . However, depending upon the beam current, power supply limits, etc., it may be desirable to set the gap such that the beam will not strike the plates before the beam reaches the slit, even at full translation. Assuming the beam entering the first translator is diverging at an opening angle of $\Delta\theta_i$, and that the beam size at entry is small compared to the gap, this constrains g as

$$g \geq 2L \tan(\Delta\theta_i). \quad (3)$$

Similarly, the depth of the plates (into / out of plane re Fig. 2) should be set such that the beam does not extend beyond the “good field” region of the plates by the time the beam reaches the second slit:

$$D_{plate} \geq 4L \tan(\Delta\theta_i) + g/2, \quad (4)$$

assuming the emittance measurement device consists of two identical translators. The slits should not cut the beam in the non-deflected plane, so in that plane beamlets retain the full divergence of the original beam. The quantity $g/2$ represents an estimate of additional width, on the order of half the gap g , required to maintain a reasonably uniform field over the beam’s maximum extent.

Modeling

We used CST Microwave Studio [8] to model a practical translator; Figure 3 shows the geometry in perspective (a) and side (b) views of the upstream translator. Table 1 provides the physical design parameters.

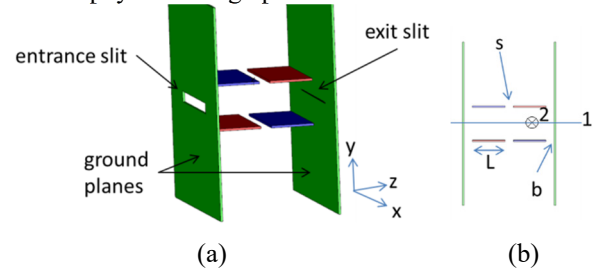


Figure 3: Translator model in (a) perspective and (b) side view. Green surfaces are held at ground; blue (red) surfaces are at positive (negative) voltages. In (b), axes 1 and 2 indicate field lineout locations.

Table 1: Electrostatic Translator Parameters

Parameter	Symbol	Value
Vertical gap	g	2 cm
Plate length	L	2 cm
Plate depth	D_{plate}	5 cm
Plate-to-plate separation	s	5 mm
Plate-to-ground plane separation	b	5 mm
Entrance slit width	w_e	5 mm
First “spatial” slit width	w_1	$5 \mu\text{m}$
Second “momentum” slit width	w_2	$20 \mu\text{m}$

Figure 4(a) and (b) show E_y along axes 1 and 2 as indicated in Figure 3(b), respectively, for the geometry shown in Figure 3 and setting $V_p = 1 \text{ V}$.

The “entrance slit” in the upstream ground plane serves, for the upstream translator, as a means for providing a field terminating surface similar to the exit plane; no beam is (ideally) lost on this plane. The emittance measurement device consists of two translators and three slits: the entrance slit, upstream translator, the “spatial” slit between the two translators, second translator, and the “momentum” slit at the exit of the second translator.

SIMULATED MEASUREMENT

The emittance measurement process was simulated using the General Particle Tracer (GPT) code [9], tracking particles from a field-emitter cathode through the emittance measurement apparatus. For the simulation, we first used a solenoidal lens as described in [6] to focus the beam to a waist inside the first translator; for a fixed beam emit-

Any distribution of this work must maintain attribution to the author(s), title of the work, publisher, and DOI.

tance, a smaller spot at the “spatial” slit increases the divergence $\Delta\theta$ of a beamlet, allowing a wider aperture at the “momentum” slit. As with any emittance measurement system, setting up the measurement device and preceding beam transport requires at least an initial estimate of the beam properties; in our case, we wished to use commercially available slits, informing our choice of focusing, waist location and spot size at the “spatial” slit.

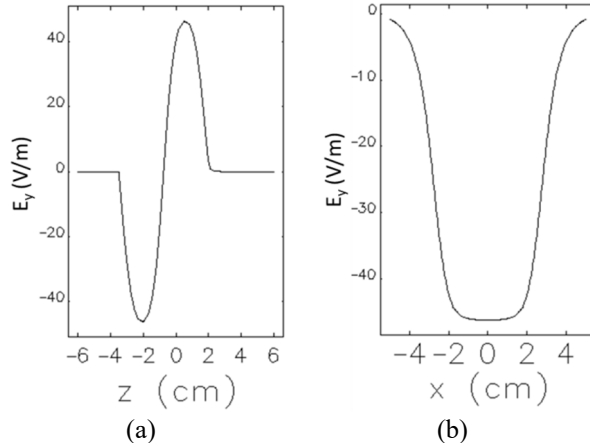


Figure 4: Field along (a) longitudinal axis and (b) transverse axis centered between two plates. (axes 1 and 2 in Fig. 3(b), respectively).

Our simulation rastered the upstream translator plate voltage by ± 230 V, and the downstream plate voltage by ± 950 V, in 27 steps per plate pair, for a total of 729 “pixels” in phase space, with each “pixel” being $5 \mu\text{m} \times 0.36$ mrad. Figure 5 shows an example of the beam propagation through the deflector plate pair during the course of the scanning process. Figure 6 shows the results of the simulated measurement.

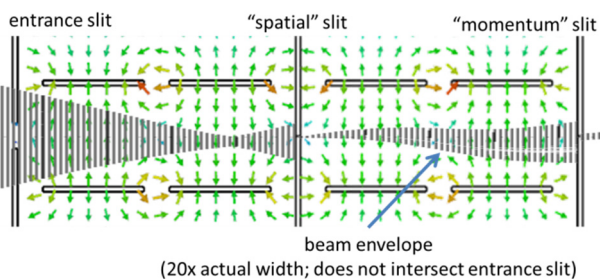


Figure 5: Beam propagation through the emittance measurement device. Arrows show electric field direction; color indicates magnitude. The vertical black lines show the transverse beam envelope scaled by a factor of 20.

The reconstruction is not perfect; the calculated emittance using the data shown in 6(b) is 13 nm-rad, while the emittance calculated directly from the particle cloud shown in 6(a) is 11 nm-rad. Accuracy can be increased by reducing slit size, but will be limited by the ability to measure the beam current transmitted through the second slit. In the above example, approximately 9% of the incoming beam, at most, was transmitted through the second slit. Given an “average” transmission of 0.5%, a 20 μA tip current would require measuring currents on the 100-nA scale, with < 10 nA resolution desired.

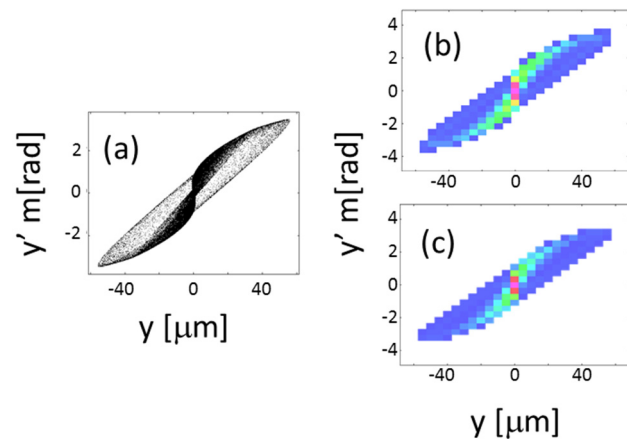


Figure 6: (a) Particle plot, (b) Reconstructed phase space, and (c) Histogram bin of 6(a), at the slit at the entrance of the “spatial slit” of the emittance measurement device.

CONCLUSION

We have designed, simulated, and will shortly begin fabricating and testing, an electrostatic two-slit emittance measurement system. Even with relatively coarse resolution, we expect to be able to resolve phase-space details and measure emittances down to 1 - 10 nm-rad using commercially available slits.

REFERENCES

- [1] E.I. Simakov *et al.*, “Diamond field emitter array cathodes and possibilities of employing additive manufacturing for dielectric laser accelerating structures,” in *AIP Conf. Proc.* **1812** (AAC2017), National Harbor, MD, Aug. 2016, doi: 10.1063/1.4975877
- [2] J.D. Jarvis *et al.*, “Uniformity conditioning of diamond field emitter arrays,” *Journ. Vac. Sci. Tech. B*, vol. 27, p. 2264, 2009, doi: 10.1116/1.3212915
- [3] H.L. Andrews *et al.*, “Current experimental work with diamond field-emitter array cathodes,” in *Proc. FEL'17*, Santa Fe, NM, USA, Aug. 2017, paper WEP015, pp. 450-453.
- [4] C.-K. Huang *et al.*, “Modeling of diamond field-emitter-arrays for high brightness photocathode applications,” in *Proc. FEL'17*, Santa Fe, NM, USA, Aug. 2017, paper WEP016, pp. 454-457.
- [5] H.L. Andrews *et al.*, “An investigation of electron beam divergence from single DFEA emitter tip,” presented at the 9th Int. Particle Accelerator Conf. (IPAC'18), Vancouver, Canada, Apr.-May 2018, paper THPML007, this conference.
- [6] R.L. Fleming *et al.*, “A simple variable focus lens for field emitter cathodes,” presented at the 9th Int. Particle Accelerator Conf. (IPAC'18), Vancouver, Canada, Apr.-May 2018, paper THPAL024, this conference.
- [7] I.V. Bazarov *et al.*, “Benchmarking of 3D space charge code using direct phase space measurements from photoemission high voltage DC gun,” *Phys. Rev. ST Accel. Beams* vol. 11, p. 100703, Oct. 2008, doi: 10.1103/PhysRevSTAB.11.100703
- [8] CST Microwave Studio, <http://www.cst.com>
- [9] General Particle Tracer, <http://www.pulsar.n1>